AAS-2007-107

ALGORITHMS FOR SAFE SPACECRAFT PROXIMITY OPERATIONS

David E. Gaylor*, Brent William Barbee†
Emergent Space Technologies, Inc., Greenbelt, MD, 20770

Future missions involving in-space servicing, repair, inspection, or rendezvous and docking require algorithms for safe, autonomous proximity operations. Algorithms for relative navigation, safe separation, and circumnavigation trajectory design are presented. The algorithms rely on safe, natural motion trajectories and covariance information from relative navigation to minimize the probability of spacecraft collision. The algorithms are described in the context of a space inspection mission where two attached spacecraft separate and one circumnavigates the other. These algorithms can also be applied to a variety of rendezvous or other proximity operations missions, whether autonomous or manually operated.

INTRODUCTION

Future spacecraft missions requiring in-space servicing, repair, inspection, or rendezvous and docking need algorithms for safe, autonomous proximity operations. Emergent Space Technologies, Inc. has developed algorithms for safe, autonomous proximity operations, including accurate relative navigation, spacecraft separation trajectory design, and circumnavigation trajectory design. The algorithms rely on safe natural motion trajectories and covariance information from the relative navigation system to minimize the probability of collision while meeting mission objectives. In this paper, we describe the algorithms in the context of a hypothetical space inspection mission where two initially attached spacecraft safely separate and then one spacecraft circumnavigates the other. The algorithms can also be applied to a variety of rendezvous missions or other missions requiring spacecraft to safely operate near each other, whether autonomous or manually operated. An example is presented in which safe natural motion trajectories are utilized to design a passively safe rendezvous trajectory for a spacecraft visiting the International Space Station (ISS).

SPACECRAFT MISSION SCENARIO

The primary and inspector spacecraft begin in a joined configuration in geosynchronous Earth orbit (GEO), with the inspector attached to the primary's outer hull. It is assumed that the primary spacecraft dos not communicate with the inspector. However, it may be possible for the inspector spacecraft to receive state information for the primary spacecraft via ground station updates. The inspector spacecraft may also be observing the primary using relative sensors, such as radar, LIDAR, or optics. Such relative measurements may include range, range-rate, and relative location angles (e.g., azimuth and elevation). If the primary spacecraft is completely non-cooperative, only relative measurements, possibly combined with absolute state updates from the ground, will be available to the inspector.

* Vice President, Aerospace Systems, Email: dave.gaylor@emergentspace.com.
† Aerospace Engineer, Email: brent.barbee@emergentspace.com.

The mission objectives are for the inspector to safely separate from the primary, circumnavigate the primary and perform inspection by traveling to six waypoints that offer views of the primary from all six faces of a virtual cube centered on the primary, and then enter into passively safe relative motion from which further inspections or other operations can be initiated, ultimately concluding with safe disposal for the inspector at the end of its mission life, which is beyond the scope of this study.

COLLISION PROBABILITY

Much work has been done to address the computing of collision probability for neighboring space objects.(Ref. 1-9) Typically, one determines if and when a secondary object will enter a user-defined safety zone. The uncertainties associated with position are represented by three-dimensional Gaussian probability densities. These densities take the form of covariance matrices which can be obtained from a sequential or batch orbit estimation process. Positions and covariance matrices are propagated to the time of closest approach and the probability of collision is usually estimated at this point.

As will be detailed in a subsequent section, the covariance information can be used to define an error ellipsoid centered at the origin of the relative motion frame, which coincides with the nominal location of the primary spacecraft's center of mass. Error ellipsoids are defined such that there is a known probability that the primary spacecraft's center of mass is within or on the surface of the error ellipsoid. If the inspector remains outside this ellipsoid then the probability of collision is less than or equal to a certain value. Keeping the inspector spacecraft outside the chosen error ellipsoid is the safety strategy employed in this paper.

RELATIVE NAVIGATION

Accurate relative navigation is a key requirement for safe spacecraft proximity operations. An extended Kalman filter (EKF) can be used onboard one or both spacecraft to estimate the absolute position and velocity of both spacecraft based on GPS, differential GPS, state updates from the ground, or relative range, range-rate, and angle sensors. The relative state estimate can be formed by taking the difference between the estimated absolute position and velocity vectors for both spacecraft.

Navigation is typically performed in the Earth-Centered Inertial (ECI) reference frame because high fidelity equations of motion are available. If relative navigation is performed in the relative motion or Hill's frame, referred to as the Radial-In-track-Cross-track (RIC) frame in this paper, only simplified equations of motion can be used.

One of the key outputs of the relative navigation system is the covariance matrix, which characterizes the uncertainty of the spacecraft position and velocity estimates. If we assume that the position errors are uncorrelated, the 3×3 sub-matrices of the covariance matrix associated with the inertial position vectors of each spacecraft can be added together, resulting in the Joint Covariance Matrix (JCM). The JCM is used to generate an error ellipsoid centered on the primary spacecraft. This error ellipsoid is computed such that the center of mass of the primary spacecraft is within or on the surface of the ellipsoid with probability $1-P_c$, where P_c is the desired maximum probability of collision. Hence, if the desired P_c is 2 % then the error ellipsoid about the primary spacecraft is computed such that the primary is known to be within or on the surface of the ellipsoid with 98% certainty. Figure 1 shows the dimensions of an error ellipsoid in its principal frame and the same ellipsoid in its orientation in the RIC frame. The error ellipsoid is always centered at the origin of the RIC frame, where the center of mass of the primary spacecraft is nominally located.

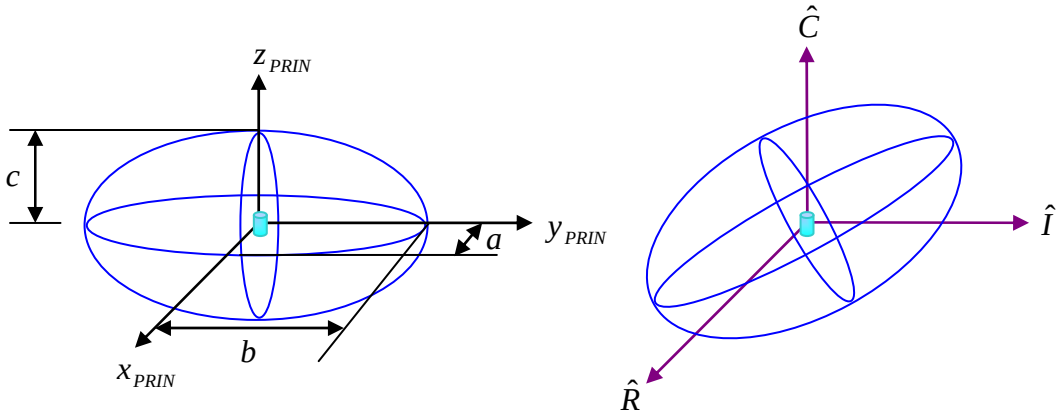

Figure 1 – Error Ellipsoid in the Principal Frame and in the RIC Frame

The parameter σ is the standard deviation of the error ellipsoid. This value must be chosen to correspond to $1-P_c$ according to Eq. (1). (Ref. 9)

$$(1-P_c) = erf\left(\frac{\sigma}{\sqrt{2}}\right) - \left[\sigma\left(\sqrt{\frac{2}{\pi}}\right)e^{\frac{-\sigma^2}{2}}\right] \tag{1}$$

Thus if P_c is 2% or 0.2, $1-P_c$ is equal to 0.98, and Eq. (1) is solved for this value. Since Eq. (1) cannot be solved analytically, an efficient adaptive solver algorithm was written that brackets the interval on which σ lies and then samples the interval at an adaptive resolution until σ is found within a specified tolerance. This value of σ is then used to compute the error ellipsoid dimensions. For a P_c of 2%, σ is 3.1365.

SAFE SPACECRAFT SEPARATION

The inspector spacecraft must safely separate from the primary in order to begin mission operations. The separation may be accomplished using a spring or other mechanism to provide the inspector spacecraft with its initial relative velocity for separation, $\Delta\vec{v}_{SEP}$. Figure 2 illustrates the configuration at the time of separation.

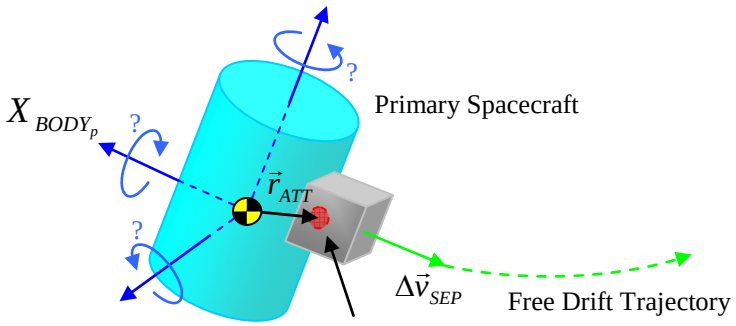

Figure 2 – Spacecraft Configuration at the Time of Separation

The inspector spacecraft is attached to the outer hull of the primary at some attachment point and the primary spacecraft's body frame is at some orientation with respect to the RIC frame and possibly rotating as well, as shown in Figure 2,. The separation impulse, $\Delta\vec{v}_{SEP}$, is therefore a function of the primary's orientation, the characteristics of the deployment mechanism (e.g., spring constant), and the primary's attitude and attitude rates.

The magnitude of $\Delta\vec{v}_{SEP}$ is determined by the characteristics of the deployment mechanism and the mass of the inspector spacecraft. The orientation of $\Delta\vec{v}_{SEP}$ is dictated at any instant in time by the orientation of the primary. The angular velocity of the primary, if any, also contributes to $\Delta\vec{v}_{SEP}$. We assume that it is possible to specify an orientation and angular velocity for the primary at the time of separation and thus are able to choose the direction of $\Delta\vec{v}_{SEP}$. We further assume in this study that the primary has zero angular velocity, though the analysis that follows is easily modified to include a non-zero angular velocity for the primary, as shown in Eq. (3).

Figure 3 illustrates the orientation of $\Delta\vec{v}_{SEP}$ in terms of two spherical coordinate angles, α (azimuth) and δ (elevation). The objective of the safe separation study is to choose the azimuth and elevation that maximize the closest approach distance between the inspector and the primary over 7 days.

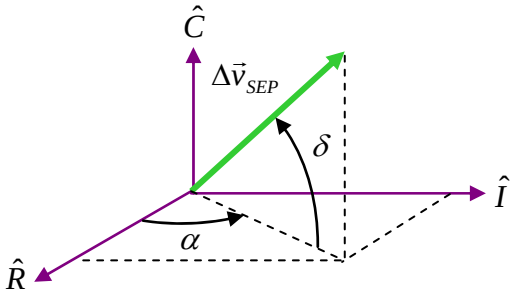

Figure 3 – Separation Maneuver Parameterization

Evaluation of the objective function given in Eq. (4) requires propagation of the equations of motion for both spacecraft. The inertial initial position vector for the inspector spacecraft is given in Eq. (2) and the initial velocity vector, including a non-zero angular velocity vector for the primary spacecraft and the separation maneuver, is specified in Eq. (3).

$$\vec{r}_{i_{ECI}}\left(t_0\right) = \vec{r}_{p_{ECI}}\left(t_0\right) + T_{ECI}^{BODY}\vec{r}_{ATT_{BODY}} \tag{2}$$

$$\vec{v}_{i_{ECI}}\left(t_0\right) = \vec{v}_{p_{ECI}}\left(t_0\right) + \left(\vec{\omega}_{BODY/ECI} \times \vec{r}_{ATT_{BODY}}\right) + T_{ECI}^{RIC}\Delta\vec{v}_{SEP_{RIC}} \tag{3}$$

$$P = \min\left(\left\|\vec{r}_{p_{ECI}}\left(t\right) - \vec{r}_{i_{ECI}}\left(t\right)\right\|\right) \tag{4}$$

Since evaluation of P requires the numerical integration of the orbital equations of motion for both spacecraft using dynamics models of adequate fidelity, the problem of maximizing P does not lend itself to analytical optimization methods. While numerical optimization methods exist that may be able to determine the optimal (α,δ) in less time than is required to map out the entire solution space methodically, knowing the sensitivity of the optimal solution to changes in (α,δ), as well as the ranges of (α,δ) that meet the probability of collision requirements, is important since in practice the exact optimal values will never be perfectly realized and there may be limitations on the available orientations for the primary spacecraft. Therefore the entire solution space for P is mapped out as a function of (α,δ) and presented in Figure 4. From Figure 5 it is clear that there is a globally optimal solution and a spread of solutions that are still advantageous.

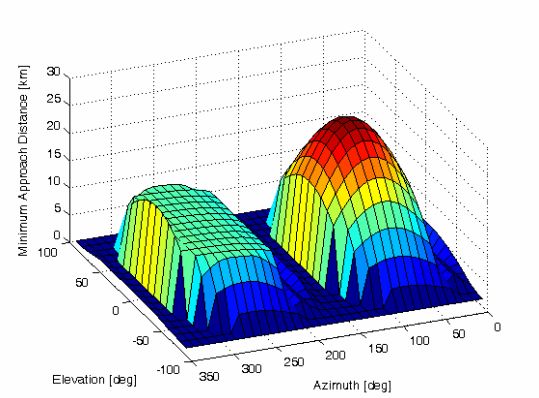

Figure 4 – Three Dimensional Performance Index Surface in Azimuth-Elevation Space

The primary and inspector spacecraft begin collocated in GEO. The optimal solution for a Δv_{SEP} of 0.1 m/s is α = 90°, δ = 0°, and the associated maximum minimum approach distance over 7 days is 26.52 km.

SAFETY ELLIPSE THEORY

A "safety ellipse" is an out-of-plane elliptical periodic relative motion trajectory around the primary spacecraft such that the trajectory never crosses the velocity vector of the primary. In a safety ellipse trajectory, drift of the two spacecraft, due to relative state estimation errors or other problems, will not result in collision, so the trajectory is considered passively safe. (Ref. 10)

A safety ellipse may be centered on the primary spacecraft (the origin of the RIC frame) or another point along the primary spacecraft in-track direction. A safety ellipse may remain stationary (static) or it may drift along the in-track direction. A safety ellipse that drifts along the in-track axis is called a "walking safety ellipse" (WSE). Examples of centered and offset static safety ellipses are shown in Figure 5. Note that safety ellipses are always rotated out of the primary spacecraft's orbit plane and are always rotated solely about the radial axis. By definition a safety ellipse may never have a rotation angle of 0° or 90° about this axis.

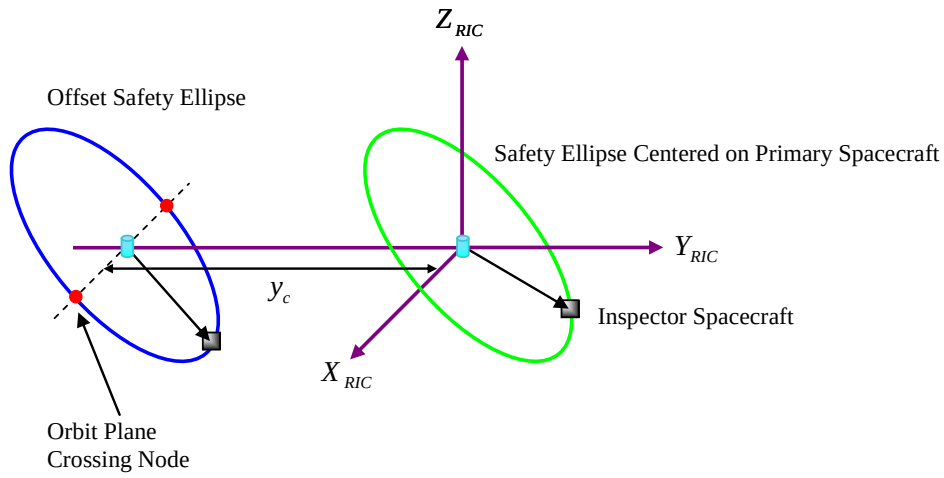

Figure 5 – Primary-Centered and Offset Static Safety Ellipses

A dynamical derivation of the safety ellipse equations of motion is found in Ref. 10. However, we present a geometrical approach to illustrate key features of the safety ellipse relevant to safe circumnavigation trajectory design. This geometrical approach permits derivation of the equations of

motion for centered and offset static safety ellipses but does not lead directly to the full equations of motion that also describe WSEs.

To begin, we define a safety ellipse reference frame where the X_E and Y_E axes lie in the plane of the safety ellipse. This reference frame is rotated by an angle θ with respect to the RIC frame and this is depicted in Figure 6a. Figure 6b shows the plane of the safety ellipse motion and introduces a polar angle in this plane, referenced to the X_E axis, denoted by χ. This polar angle specifies the location of the inspector spacecraft on the safety ellipse at any time.

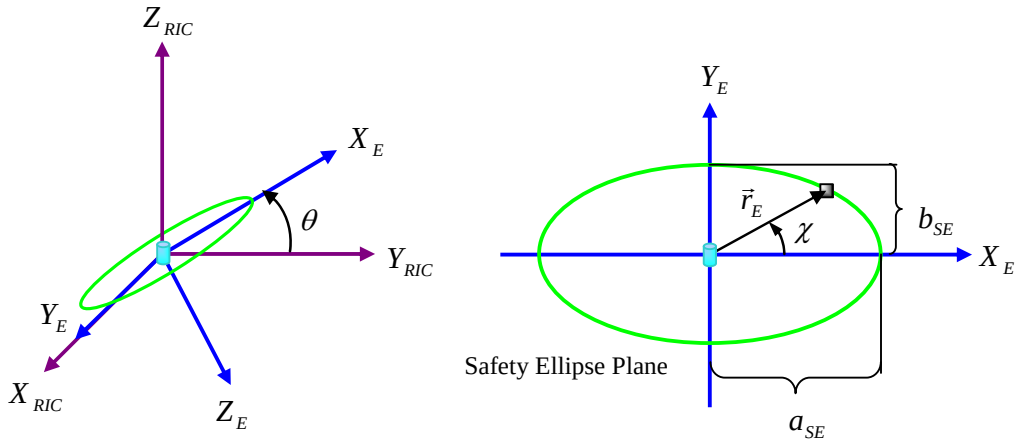

(a) **(b)**

Figure 6 – (a) Safety Ellipse Reference Frame and (b) Safety Ellipse Plane with Polar Angle

Noting also the semi-axis lengths of the safety ellipse, a_{SE} and b_{SE}, it is possible to write the position vector of the inspector in the safety ellipse frame, given in Eq. (5).

$$\vec{r}_E = \begin{bmatrix} x_E \\ y_E \\ z_E \end{bmatrix} = \begin{bmatrix} a_{SE}\cos(\chi) \\ b_{SE}\sin(\chi) \\ 0 \end{bmatrix} \tag{5}$$

Since the Y_E axis is aligned with the X_{RIC} axis, as seen in Figure 6a, it is clear that the semi-minor axis of the safety ellipse is the maximum distance of the inspector spacecraft along the X_{RIC} axis, denoted as $x_{\max}$. This condition is expressed in Eq. (6).

$$b_{SE} = x_{\max} \tag{6}$$

To express the RIC position vector of the inspector spacecraft along the safety ellipse, it is necessary to develop the transformation between the RIC and safety ellipse frames. Figure 9 illustrates the necessary rotation about the X_{RIC} axis by θ and shows the basis vector correspondences. Examination of Figure 7 leads to the matrix that transforms vectors between the RIC frame and the safety ellipse frame, presented in Eq. (7).

$$T_{RIC}^{E} = \begin{bmatrix} 0 & 1 & 0 \\ \cos(\theta) & 0 & \sin(\theta) \\ \sin(\theta) & 0 & -\cos(\theta) \end{bmatrix} \tag{7}$$

Substituting Eq. (6) into Eq. (5) and then multiplying by Eq. (7) leads to the RIC position vector for the inspector spacecraft, given in Eq. (8).

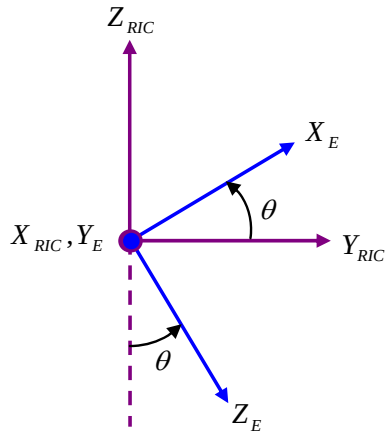

Figure 7 – Rotation between the RIC Frame and the Safety Ellipse Frame

Note that the RIC position vector for the inspector spacecraft in Eq. (16) is parameterized by the safety ellipse polar angle, the angle by which the safety ellipse is rotated out of the primary's orbit plane, the maximum radial axis extent of the safety ellipse, and the semi-major axis of the safety ellipse. It is desirable to find a means to remove the dependence on the safety ellipse semi-major axis so that the position vector consists solely of terms that are related directly to the RIC frame.

$$\vec{r}_{RIC} = T_{RIC}^{E}\vec{r}_{E} = \begin{bmatrix} x_{\max}\sin(\chi) \\ a_{SE}\cos(\chi)\cos(\theta) \\ a_{SE}\cos(\chi)\sin(\theta) \end{bmatrix} \tag{8}$$

This is accomplished by examining a view of the safety ellipse edge-on in the In-track-Cross-Track plane of the RIC frame, shown in Figure 8.

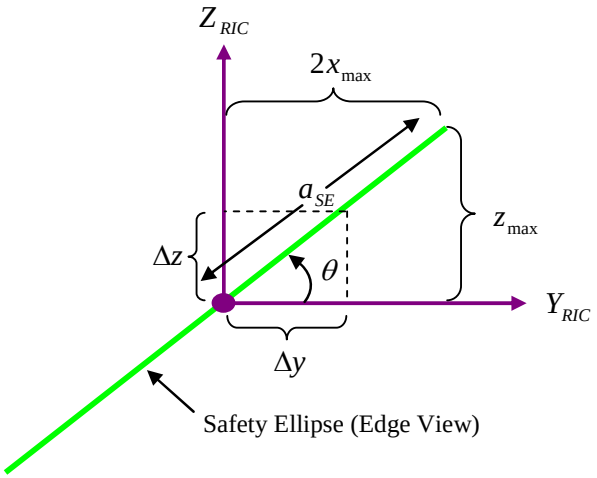

Figure 8 – In-track-Cross-Track View of the Safety Ellipse, Edge-On

In Figure 8 the rotation angle θ appears, along with a new quantity, $z_{\max}$, which is the maximum extent of the safety ellipse motion along the Z_{RIC} axis. Figure 10 illustrates the desired relationships between the safety ellipse semi-major axis, $x_{\max}$, and $z_{\max}$, shown in Eqs. (9).

$$
\begin{aligned}
a_{SE}\cos(\theta) &= 2x_{\max} \\
a_{SE}\sin(\theta) &= z_{\max}
\end{aligned}
\tag{9}
$$

Substituting Eqs. (9) into Eq. (8) yields Eqs. (10), which specify the position of the inspector spacecraft in the RIC frame solely as a function of the safety ellipse motion plane polar angle, χ, noting that $x_{\max}$ and $z_{\max}$ are constants. Note also that the term y_c is added to the y RIC coordinate to allow the construction of the offset static safety ellipses mentioned previously. A non-zero y_c allows the center of the safety ellipse to be positioned anywhere along the In-track axis.

$$
\begin{aligned}
x(\chi) &= x_{\max}\sin(\chi) \\
y(\chi) &= 2x_{\max}\cos(\chi) + y_c \\
z(\chi) &= z_{\max}\cos(\chi)
\end{aligned}
\tag{10}
$$

The RIC velocity of the inspector spacecraft on the safety ellipse is computed by taking the first time derivative of Eqs. (10), but first the time dependence of the polar angle must first be specified. Since the period of the safety ellipse motion is equal to the period of the primary spacecraft's orbit, the time dependence of the polar angle depends on the mean motion, n, of the primary, as shown in Eq. (11) (Ref. 2).

$$
\chi(t) = n\left(t - t_{\chi=0}\right) \tag{11}
$$

Thus, taking the first time derivative of Eqs. (10) yields the inspector spacecraft RIC velocity, given in Eqs. (12).

$$
\begin{aligned}
\dot{x}(\chi) &= x_{\max} n\cos(\chi) \\
\dot{y}(\chi) &= -2x_{\max} n\sin(\chi) + \dot{y}_c \\
\dot{z}(\chi) &= -z_{\max} n\sin(\chi)
\end{aligned}
\tag{12}
$$

Eqs. (10) and (12) are the equations of motion for centered and offset static safety ellipses. To arrive at the complete safety ellipse equations of motion that also account for WSEs, period-matching constraints and phase space analyses are invoked (Ref. 2) and this derivation is omitted here for brevity. The full safety ellipse equations of motion are presented in Eqs. (13) (Ref. 6).

$$
\begin{aligned}
x(\chi) &= x_{\max}\sin(\chi) - \frac{2\dot{y}_c}{3n} \\
y(\chi) &= 2x_{\max}\cos(\chi) + \frac{\dot{y}_c\left(\chi - \pi/2\right)}{n} + y_c \\
z(\chi) &= z_{\max}\cos(\chi) \\
\dot{x}(\chi) &= x_{\max} n\cos(\chi) \\
\dot{y}(\chi) &= -2x_{\max} n\sin(\chi) + \dot{y}_c \\
\dot{z}(\chi) &= -z_{\max} n\sin(\chi)
\end{aligned}
\tag{13}
$$

It is of interest to note that the safety ellipse motion plane polar angle, χ, also arises in the dynamical derivation of safety ellipse motion as the X_{RIC} phase space angle. The dynamical derivation also references the Z_{RIC} phase space angle, denoted as γ, and Eq. (14), which is the core safety ellipse criterion, makes it clear that γ is also a safety ellipse motion plane polar angle.

$$\psi = \chi - \gamma = \frac{\pi}{2} \tag{14}$$

Thus χ (and γ) have meaning in both phase space and Euclidean space. In terms of the safety ellipse equations of motion presented in Eqs. (13), we find it most instructive to think of χ as the safety ellipse motion plane polar angle and this is the motivation for the presentation of the geometrical derivation of the equations of motion in lieu of the dynamical derivation. WSE motion is shown from a perspective view in Figure 8 and in the RIC planes in Figure 9.

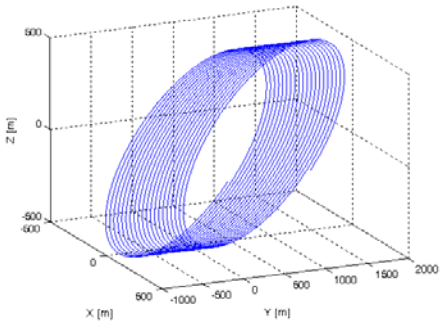

Figure 8- Perspective View of Walking Safety Ellipse Motion

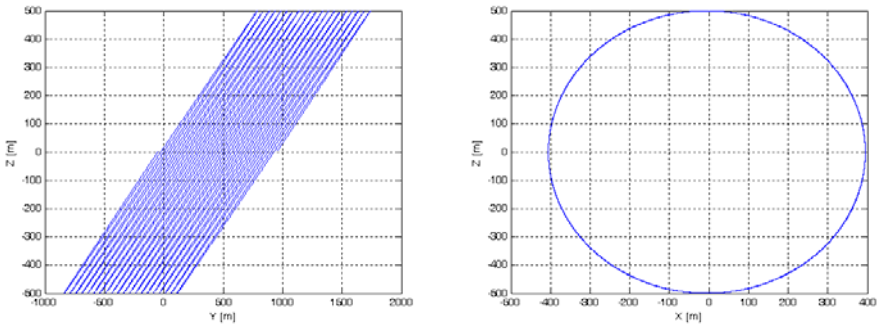

Figure 9 – (a) In-track-Cross-Track View of a Walking Safety Ellipse and (b) Radial-Cross-Track View of a Walking Safety Ellipse

Note that the WSE forms a tubular manifold around the in-track axis. This fact will be utilized in the safe circumnavigation trajectory design presented in a subsequent section.

Injection onto a safety ellipse is possible in one of two modes. In the first mode the position vector of the inspector spacecraft already corresponds to a safety ellipse and a simple velocity change maneuver accomplishes the injection. In the second mode the inspector spacecraft's position does not satisfy the safety ellipse position equations and so the inspector must perform a maneuver to transfer to a viable injection point and then perform a second velocity change maneuver to achieve injection.

One means of achieving injection is summarized by Eqs. (15) and Eq. (16).

$$\begin{aligned} \Delta x &= x - \left(x_{\max} \sin(\chi) - \frac{2\dot{y}_c}{3n} \right) \\ \Delta y &= y - \left(2x_{\max} \cos(\chi) + \frac{\dot{y}_c \left(\chi - \pi/2 \right)}{n} + y_c \right) \\ \Delta z &= z - \left(z_{\max} \cos(\chi) \right) \end{aligned} \tag{15}$$

$$\Delta r = \sqrt{\Delta x^2 + \Delta y^2 + \Delta z^2} \tag{16}$$

In Eqs. (15), x, y, and z are the RIC position coordinates of the inspector spacecraft at the time at which it is desired to injection onto a safety ellipse. Eq. (16) expresses the distance between the inspector spacecraft and the nearest viable injection point and this equation is numerically minimized to determine the closest available injection point. In the case where the inspector is already at a viable injection point, the minimum of Eq. (16) is zero. If the minimum Δr is greater than zero, time of flight along the trajectory to the injection must be chosen and a maneuver computed. Upon arrival at the injection point, the injection maneuver itself is performed.

A numerical optimizer can be used to solve for the set of safety ellipse parameters $\{x_{\max}, z_{\max}, \chi, y_c, \dot{y}_c\}$ that minimizes Eq. (16). These parameters may all be left free, or some may be specified a priori. In either case, once the safety ellipse parameters have been computed, the position of the injection point is specified by the position portion of Eqs. (13) if it does not coincide with the inspector's current position and the required velocity at the injection point is given by the velocity portion of Eqs. (13). If $\vec{v}_{CURR}$ is the inspector's velocity vector at the time of arrival at the injection point, then the injection maneuver is given by Eq. (17).

$$\Delta\vec{v}_{INJECT} = \vec{v}_{SE} - \vec{v}_{CURR} \tag{17}$$

CIRCUMNAVIGATION TRAJECTORY DESIGN

Circumnavigation of the primary by the inspector requires the inspector to travel to six waypoints. Each of the six waypoints lies on the face of a virtual cube centered on the nominal position of the primary. These six points are also the vertices of an octahedron centered on the primary such that the octahedron is circumscribed by the virtual cube. Although attitude dynamics are not modeled, it is assumed that the inspector continually performs attitude maneuvers that keep the inspection sensor pointing inward and directly at the primary while the circumnavigation is performed as the inspector visits each of the six waypoints in turn.

The design of the circumnavigation trajectory segments includes considerations for safety as well as the total Δv required to complete the circumnavigation. In particular, a waypoint range, R_{WP}, and Time of Flight (TOF) per trajectory segment will be chosen. It is assumed in this study that the TOF is the same for all trajectory segments. R_{WP} is chosen to satisfy safety requirements and an algorithm is described that allows the selection of the TOF to satisfy total Δv requirements. Figure 10 depicts the circumnavigation octahedron for which the waypoints all lie on the RIC axes.

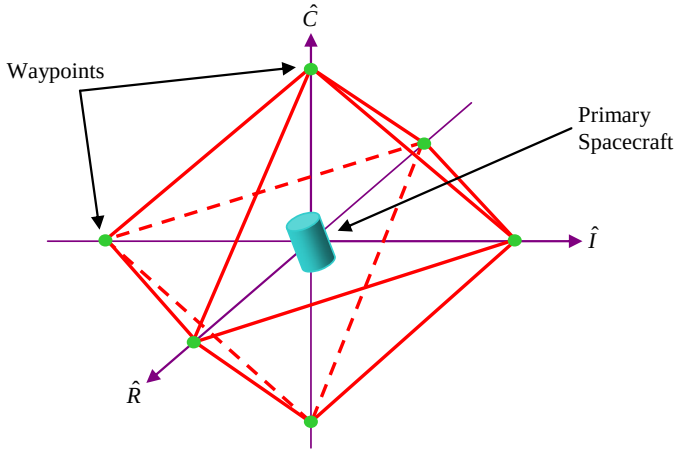

Figure 10 – Prototypical Circumnavigation Octahedron

The octahedron is transformed into a Safety Octahedron such that none of the octahedron's edges (possible trajectory segments) cross the primary spacecraft's velocity vector. The SO, shown in Figure 11, also has the property that all the waypoints lie on the surface of a WSE manifold.

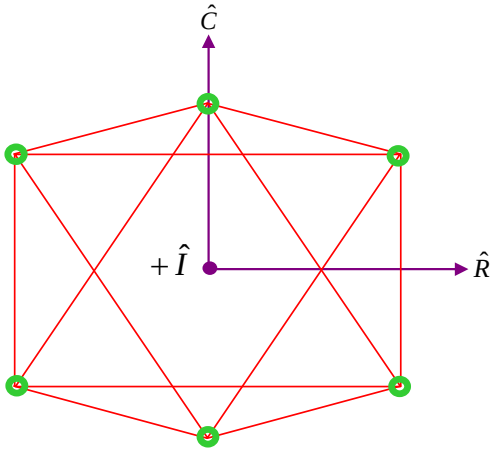

Figure 11 – Radial-Cross-Track View of a Safety Octahedron

WAYPOINT TRAVERSAL ORDERING

This study determined that there is a minimum total Δv waypoint traversal order and that this order is independent of both the waypoint range and the TOF per trajectory segment. However it was found that the minimum Δv order does depend on the orientation of the SO, meaning that the minimum Δv waypoint order analysis must be performed each time the orientation of the SO changes. This also means that the minimum Δv waypoint order can be selected prior to the final determination of waypoint range or TOF per trajectory segment. The parameter to be minimized is the total Δv for the circumnavigation sequence, given in Eq. (18), where N is the number of waypoints and the subscript i references a particular waypoint.

$$\Delta v_{TOTAL} = \sum_{i=1}^{N-1} \left\| \Delta \vec{v}_{i \to i+1} \right\| \tag{18}$$

The minimum Δv waypoint order analysis consists of computing the total Δv required for each permutation of waypoint order. The set of permutations considered is formed subject to the following constraints: first, no trajectory segment is allowed to pass through the origin and second, in the case where the inspector spacecraft returns to the first waypoint (a "closed" trajectory sequence), waypoints are not allowed to repeat. Results for the non-closed trajectory sequence are presented in this section and the results have the same character for the closed sequence. In the non-closed case the inspector simply visits all six waypoints and does not return to the first waypoint. The results of scanning all waypoint order permutations are presented in Figure 12.

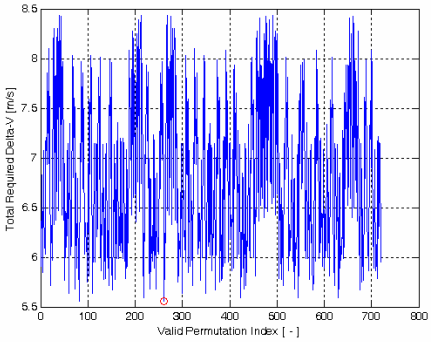

Figure 12 – Total Circumnavigation Δv for each Viable Waypoint Order Permutation

While the number of viable permutations is large, on the order of hundred or thousands, a typical modern desktop computer can sample them all in a matter of seconds. Although it is not necessary to compute the waypoint range and TOF prior to performing the optimal waypoint analysis, doing so illustrates the difference between the maximum and minimum total Δv, quantifying the benefit of using the optimal order. For this example, a waypoint range of 678.2 m and a TOF per trajectory segment of 1200 seconds were used. Figure 16 shows that the total Δv for the worst waypoint order is 8.43 m/s and the Δv for the optimal waypoint order is 5.56 m/s, a reduction of approximately 34% from the worst case. The optimal waypoint order is given in Table 1 along with the original waypoint order on the prototypical octahedron. Note that transformation of the prototypical octahedron to a SO does not change the waypoint order.

Table 1 – Optimal Waypoint Order and Original Waypoint Order for Prototypical Octahedron

Optimal Waypoint Order	Original Waypoint Order	Waypoint Locations on Prototypical Octahdron
4	1	$+x$, 0, 0
5	2	$-x$, 0, 0
1	3	0, $+y$, 0
2	4	0, $-y$, 0
3	5	0, 0, $+z$
6	6	0, 0, $-z$

WAYPOINT RANGE SELECTION

The selection of waypoint range is typically a trade-off between safety and sensor performance. The waypoint range also affects the total Δv required to complete the circumnavigation sequence. We will examine the selection of waypoint range solely to ensure safety. Total Δv requirements will be met by selecting the TOF per trajectory segment.

The waypoint range is shown graphically in Figure 13a. In order to meet a safety requirement that P_c is kept to a maximum of 2%, we circumscribe a sphere, termed the Safety Sphere (SS) around the 3.1365σ error ellipsoid, recalling that this error ellipsoid is derived such that there is a 98% certainty that the primary spacecraft's center of mass is within or on the surface of this ellipsoid. We then circumscribe the SO about the SS, which means that none of the possible trajectory segments (octahedron edges) will penetrate the SS and hence never penetrate the 98% error ellipsoid, thus satisfying the requirement that P_c is ≤ 2 %.

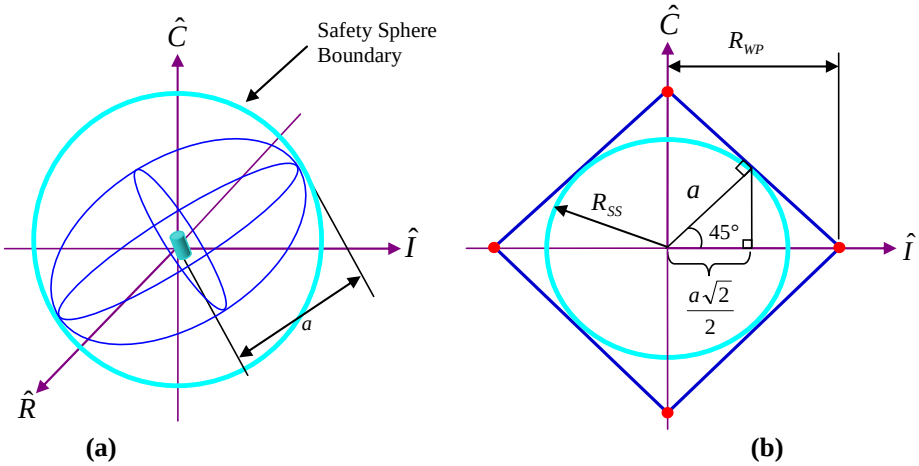

Figure 13 – (a) Safety Sphere Circumscribing the Error Ellipsoid About the Primary Spacecraft and (b) Planar View of Safety Octahedron Circumscribing the Safety Sphere

Figure 13b shows a planar view of the SO circumscribed about the SS and shows the computation of the waypoint range as a function of the radius of the SS, which is equal to the longest axis, a, of the error ellipsoid. The relationship between the waypoint range and a is illustrated in Figure 13b and expressed in Eq. (30).

$$R_{WP} = a\sqrt{2} \tag{19}$$

The waypoint range is modified such that it accounts for the extent of the physical structure of both spacecraft as well as a selectable margin of safety, as shown in Figure 14.

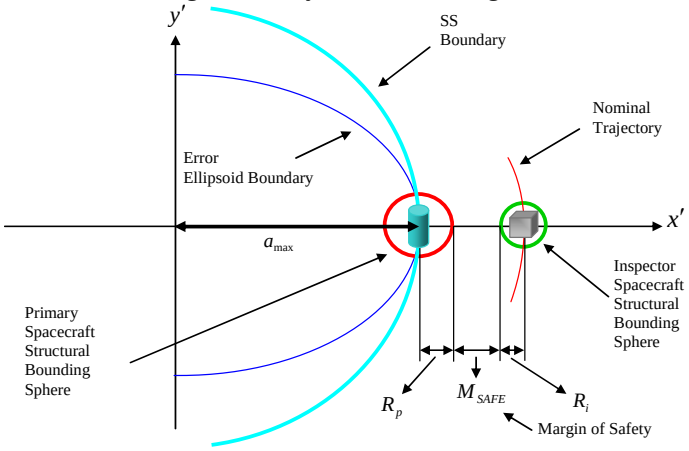

Figure 14 – Waypoint Range Augmentation

Eq. (20) expresses the waypoint range as a function of the longest error ellipsoid axis, the structural bounding spheres around both spacecraft, and the selected margin of safety.

$$R_{WP} = \left(a_{\max} + R_p + M_{SAFE} + R_i\right)\sqrt{2} \tag{20}$$

For the example circumnavigation results that are presented in a subsequent section, a sample covariance matrix was formed and values of 3, 0.5, and 10 m were chosen for R_p, R_i, M_{SAFE}, respectively. The resulting waypoint range is 678.2 m. It is of note that when circumscribing a sphere around the error ellipsoid, empty volume remains between the ellipsoid and the sphere that could theoretically be utilized but isn't. If the error ellipsoid is too oblong this volume of unused but theoretically safe space between the ellipsoid and the sphere becomes rather large and it may be desirable to take another approach to safety that the does not force the inspector spacecraft unnecessarily far from the nominal location of the primary. One possible approach is to rotate the SO such that the oblong ellipsoid passes through the SO without crossing any possible trajectory segments, as shown in Figure 15. This reorientation of the SO may cause one of the possible trajectory segments to cross or nearly cross the primary's velocity vector, which is contrary to the definition of the SO, so this possibility must be balanced against the benefits of reorienting the SO to pass around the very oblong ellipsoid. The primary benefit is that the inspector spacecraft can get much closer than it could otherwise to the primary while still maintaining the desired probability of collision.

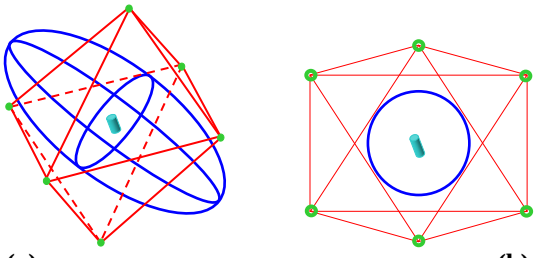

(a) **(b)**

Figure 15 – (a) Perspective View and (b) Planar View of Safety Octahedron Reoriented to Pass around a Very Oblong Error Ellipsoid

TIME OF FLIGHT (TOF) SELECTION

An algorithm has been developed to determine the TOF and the waypoint range that satisfy a given total Δv requirement for the circumnavigation sequence. This is useful for keeping the total fuel usage for circumnavigation at an achievable level and for providing a means to select TOF. The only other relevant effect of TOF is the curvature of each trajectory segment; the longer the TOF, the more each trajectory segment deviates from a straight line between waypoints.

The two main inputs to the algorithm are a vector of TOFs and a vector of waypoint ranges. In the case where the waypoint range has already been chosen for safety, this single chosen waypoint range replaces the vector of waypoint ranges, reducing the design space from two dimensions to one. Additionally the target total Δv is provided, along with a tolerance. The final inputs are a desired waypoint range (if the waypoint range is left free) and a desired TOF. The algorithm forms the design space and adaptively scans it until finding at least one solution that meets the target total Δv within tolerance. If more than one solution is found, the system indicates which solution is closest to the desired TOF and waypoint range. Total Δv is computed via Eq. (18), as previously discussed in the section on optimal waypoint ordering. Example system output is shown in Figures 16a and b. Figure 16a shows the output when the design space only consists of TOF (waypoint range is already chosen) and Figure 16b shows the output when the design space consists of both TOF and waypoint range.

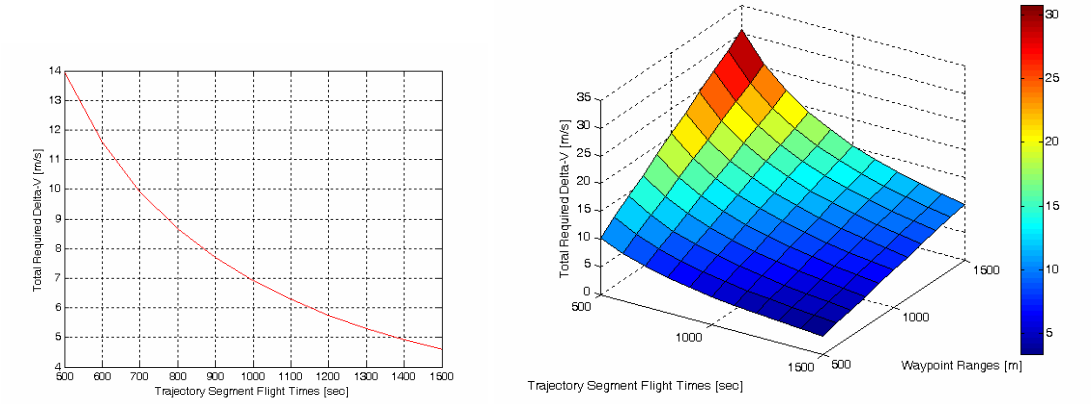

(a) **(b)**

Figure 16 – Algorithm Output for (a) TOF Only and (b) for TOF and Waypoint Range

In Figure 16a the waypoint range has been fixed at 678.2 m and the curve shows total Δv as a function of TOF in seconds. The algorithm was given a target total Δv of 5 ± 1 m/s and determined that the closest solution is a TOF of 1200 sec, which yields a total Δv of 5.75 m/s. This Δv is reduced to 5.56 m/s once the optimal waypoint order is determined, as described in a previous section. The computed TOF of 1200 seconds per trajectory segment will be utilized in the subsequent section in which the simulation results for an example circumnavigation mission are presented.

In Figure 16b the same parameters are used except that a vector of waypoint ranges is provided. The resulting solution surface is a slightly warped plane of total Δv values.

FITTING SAFETY OCTAHEDRON WAYPOINTS TO A WALKING SAFETY ELLIPSE

Given the orientation of a safety octahedron, it is desirable to place the waypoints on a WSE manifold. From Figure 8 it is clear that WSE motion forms a tubular manifold around the in-track axis with an elliptical cross-section. It is possible to compute WSE parameters and slightly modify the waypoint range such that, for the particular safety octahedron orientation, all the waypoints lie on a WSE manifold. This allows the inspector spacecraft to directly inject onto the WSE from any waypoint. Figure 17 (not to scale) illustrates the relevant geometries.

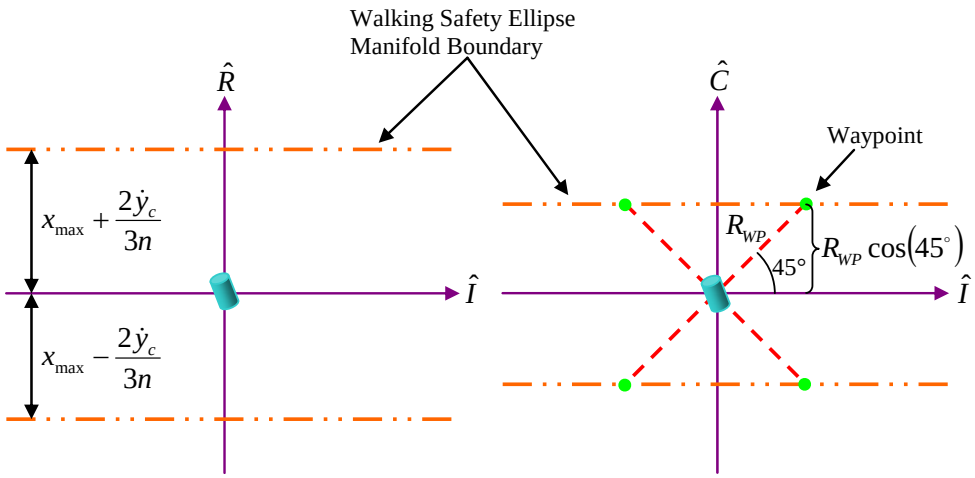

Figure 17 – Geometric Relationships to Walking Safety Ellipse Manifold Boundary

One of the key concepts illustrated in Figure 17 stems directly from the x position equation in Eqs. (13), which is that $\dot{y}_c$ is not zero because a WSE is being considered and this introduces a bias in the x direction that must be accounted for. First the waypoint range is extended by a small but comfortable margin in anticipation of the entire assembly of waypoints shifting in the radial direction, and this is shown in Eq. (21). Note that the waypoint range computed in previous sections, 678.2 m, included the small effect shown in Eq. (21).

$$R_{WP} = R_{WP} + \left| \frac{4\dot{y}_c}{n} \right| \tag{21}$$

This requires that the walk rate of the WSE must be chosen ahead of time, prior to waypoint set construction. Once the waypoint range has been modified according to Eq. (21), the $x_{\max}$ parameter for the WSE is set to the negative of the waypoint range as shown in Eq. (22).

$$x_{\max} = -R_{WP} \tag{22}$$

Note that the geometry in Figure 21 indicates how to compute the appropriate $z_{\max}$ in terms of the waypoint range, given in Eq. (23).

$$z_{\max} = R_{WP}\sqrt{2} \tag{23}$$

Finally, the bias shown in Figure 17, which is due to the influence of the walk rate term in the x position equation in Eqs. (13), is applied to all waypoint coordinates as shown in Eq. (24).

$$WP_i = WP_i - \begin{bmatrix} \frac{2\dot{y}_c}{3n} & 0 & 0 \end{bmatrix}^T \tag{24}$$

The results of these calculations are a set of waypoint coordinates that are fitted to a WSE and a partial set of parameters for the WSE, these being $\{x_{\max}, z_{\max}, \dot{y}_c\}$. Thus, to inject onto the WSE from any waypoint, Eq. (16) is minimized using Eqs. (15) with the $\{x_{\max}, z_{\max}, \dot{y}_c\}$ parameters fixed to the values described in this section. The result is that the minimum of Eq. (16) is zero, meaning that the waypoint position corresponds to a location on the WSE as intended. The minimum solution consists of the χ and y_c that correspond to the waypoint that is being injected from. This χ and y_c, along with the pre-computed $\{x_{\max}, z_{\max}\}$ are used so that direct WSE injection maneuver can be computed using Eq. (17).

It is important to note that the radial bias introduced by the non-zero $\dot{y}_c$ is small and manageable when $\dot{y}_c$ is small compared to the magnitude of mean motion, n, of the primary spacecraft's orbit. Therefore care must be exercised to select a $\dot{y}_c$ that is small enough to not pull the WSE manifold's center too far off of the in-track axis since the goal is to have motion that is nominally centered about the primary spacecraft.

WAYPOINT DRIFT-OUT ANALYSIS

One possible failure mode of the inspector spacecraft is to perform a maneuver to embark upon a trajectory segment to get to the next waypoint in the sequence and afterwards lose the ability to make any subsequent maneuvers. In this case the inspector will nominally arrive at the targeted waypoint and then depart that waypoint on a free drift trajectory. While beyond the scope of this paper, waypoint drift-out analyses have been performed using the full non-linear equations of orbital motion for the safety octahedron circumnavigation described herein. It is interesting to note that because all the waypoints lie on a WSE manifold, the inspector spacecraft's state space at these points is always near WSE state space, further evidenced by how small in magnitude the WSE injection maneuvers are from these points. Figure 18 demonstrates the WSE-like nature of drift-out motion from a waypoint; this nature is present in drift-out from all waypoints.

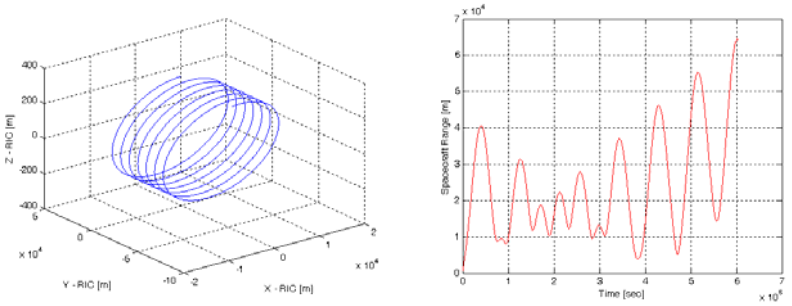

(a) **(b)**

Figure 18 – (a) Perspective View of Relative Motion and (b) Distance versus Time for 7-day Drift of Inspector from Waypoint 5 of Non-Closed Trajectory Sequence

EXAMPLE SAFE CIRCUMNAVIGATION MISSION RESULTS

A sample circumnavigation mission using a chosen covariance matrix was simulated in software using all the algorithms and parameters described thus far, along with standard Clohessy-Wiltshire (CW) targeting algorithms to demonstrate the efficacy of the techniques developed in this paper. The numerical values of the relevant parameters have been presented in their respective sections throughout this paper. Figures 19a and b present the results of the example circumnavigation mission, showing all the waypoints, all the trajectory segments, and the result of the inspector spacecraft being commanded to inject onto the WSE at waypoint 3. Additionally, a portion of the resulting WSE motion is plotted.

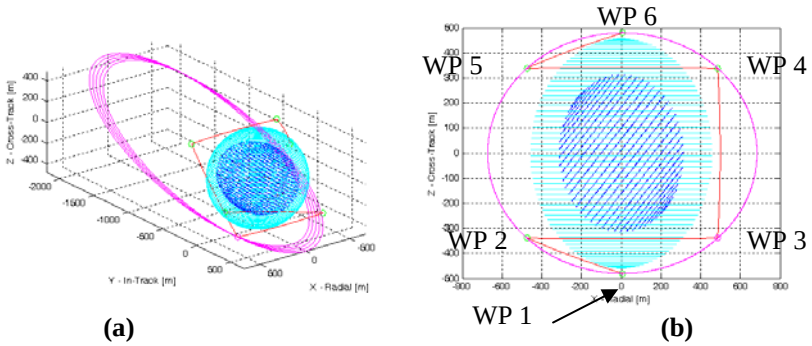

(a) **(b)**

Figure 19 – (a) Perspective View and (b) Radial-Cross-Track View of Example Circumnavigation Mission Results

From Figure 19b it is clear that all six waypoints lie on the WSE manifold as desired. Figures 19a and b together show the trajectory segments just grazing the SS, rendered in cyan, and show the SS circumscribing the error ellipsoid, rendered in blue. The WSE motion resulting from the injection at waypoint 3 result in passively safe relative motion that remains outside the SS and gradually carries the inspector away from the primary. The probability of collision, P_c, is maintained at or below the desired value of 2% since the inspector spacecraft's motion remains outside the 98% error ellipsoid.

APPLICATION OF SAFETY ELLIPSE THEORY TO RENDEZVOUS

The safety ellipse theory presented previously can also be applied to rendezvous. By approaching the destination spacecraft on a walking safety ellipse spiral, the visiting spacecraft is naturally on a passively safe approach trajectory that can be designed to respect keep-out zones around the destination. The application presented here is rendezvous with the ISS.

The visiting spacecraft begins on the In-track axis, ahead of the ISS by 15 km. The visiting spacecraft is to be transferred from that relative location to an insertion point for a -R-bar (Radial axis) final approach to the ISS in which it "hops" towards the ISS along the -R-bar. The ISS has two keep-out zones defined around it. The outermost is the Approach Ellipsoid (AE), which is a 2 km × 4 km × 2 km ellipsoid centered on the ISS with the long axis of the ellipsoid aligned with the In-track axis. The innermost zone is the Keep-Out Sphere (KOS) which has a 200 m radius and is centered on the ISS. The visiting spacecraft must remain outside the AE while it travels to the -R-bar approach insertion point. The visiting spacecraft will then penetrate the AE during the -R-bar approach and penetrate the KOS during the final 200 m of the -R-bar approach. The spacecraft positions at the time of rendezvous initiation are shown in Figure 20, along with the AE, KOS. For reference, the ISS orbit normal direction is coming directly out of the page.

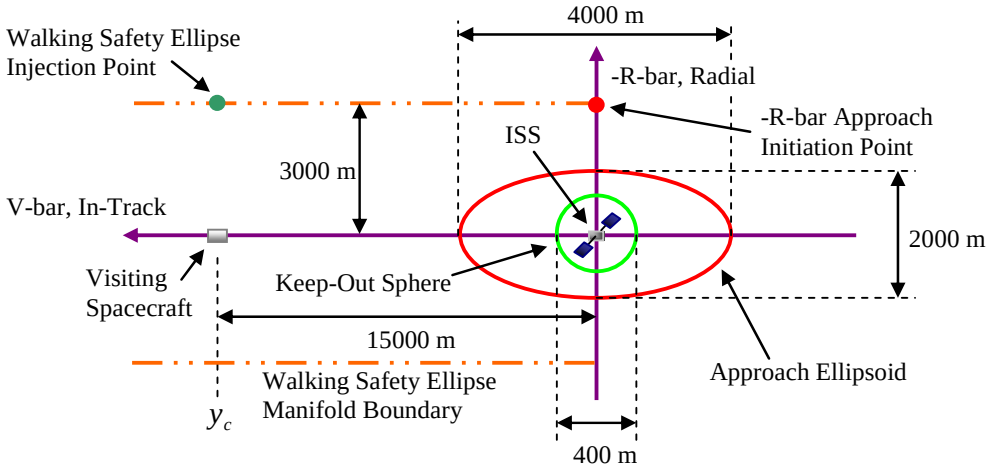

Figure 20 – Spacecraft Configuration at Time of Rendezvous Initiation (not to scale)

From Figure 20 it is clear that the WSE offset, y_c, at the WSE injection point should be equal to 15000 m. Referring back to Figures 6a and b, it is clear that the safety ellipse plane polar angle, χ, is equal to 90° at the WSE injection point. It is also clear from the x position equation in Eqs. (13) that $x_{\max}$ must be $3000 - \left|2\dot{y}_c / 3n\right|$ m, where n is equal to the mean motion of the ISS, in order for the WSE motion to intercept the -R-bar approach initiation point, which is 3000 m out along the -R-bar. The remaining safety ellipse variables to specify are either θ or $z_{\max}$ and the In-track approach rate $\dot{y}_c$.

For this example, $z_{\max}$ is chosen to be 2000 m and hence θ is 22.045°, as specified by Eq. (17). Note that $z_{\max}$ is selected to be larger than the extent of the AE by a comfortable margin so that the WSE motion

is always well outside the AE. This is also true for $x_{\max}$ though $x_{\max}$ is primarily driven by the location of the -R-bar approach initiation point (which is well outside the AE).

The In-track approach rate is selected according to the initial In-track offset distance and the desired TOF for the WSE rendezvous trajectory. In this example the desired rendezvous flight time is 3 ISS orbital periods, the In-track offset is 15000 m, as specified above, and hence the In-track approach rate is computed according to Eq. (25).

$$\dot{y}_c = -\frac{y_c}{TOF_{WSE}} \tag{25}$$

Note that the sign of Eq. (25) is determined by whether the visiting spacecraft begins ahead of or behind the ISS. Since the visiting spacecraft begins ahead of the ISS in this example ($y_c > 0$), $\dot{y}_c$ must be < 0 for rendezvous.

At this point all the safety ellipse parameters corresponding to the WSE injection point are specified, and so the RIC position coordinates of this point can be computed with the position equations in Eqs. (13). The first maneuver in the rendezvous sequence is thus a maneuver computed using CW targeting that takes the visiting spacecraft from the initial position on the V-bar to the WSE injection point. For this initial transfer, the TOF chosen for this example is ¼ of an ISS orbit.

The second maneuver injects the visiting spacecraft onto the WSE, where it will passively remain safely outside the AE as it spirals around the V-bar, bringing it to the -R-bar approach initiation point 3 ISS orbits later. The maneuver changes the visiting spacecraft's RIC velocity vector from its magnitude and direction at the WSE injection point to the required safety ellipse velocity vector specified by Eqs. (16) and (17). Upon arrival at the -R-bar approach initiation point, a series of small maneuvers are made to gently guide the visiting spacecraft down the -R-bar towards the ISS.

The advantage of this rendezvous strategy is that the trajectory always passively remains outside the AE. Thus if the visiting spacecraft suffers a system failure that renders it incapable of making subsequent maneuvers after injecting onto the WSE, it will continue to remain outside the AE, precluding a collision with the ISS at any future time. The complete set of rendezvous trajectories in simulation are shown in Figures 21 and 22a and b.

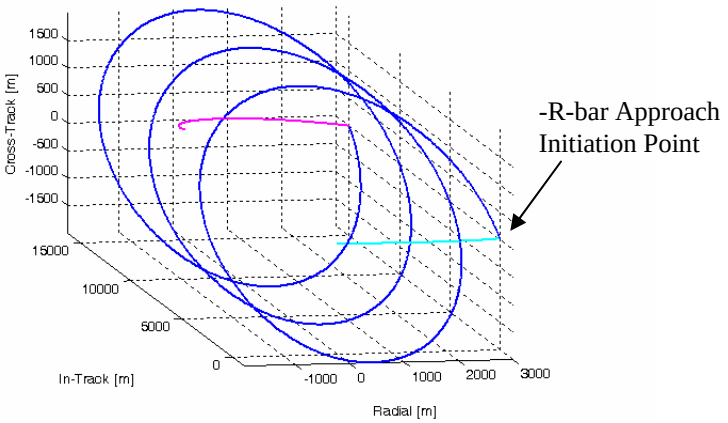

Figure 21 – Walking Safety Ellipse Rendezvous Simulation Results, Perspective View

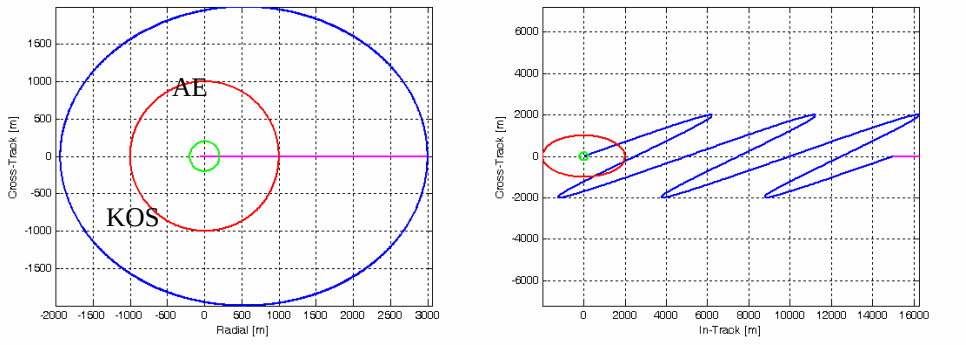

(a) **(b)**

Figure 22 – Walking Safety Ellipse Rendezvous in (a) the Radial-Cross-Track Plane and (b) the In-track-Cross-Track Plane

The typical -R-bar rendezvous scenario has the visiting spacecraft flying trajectories solely in the orbit plane and requires a total Δv of 29.4 m/s. The walking safety ellipse rendezvous presented here requires a total Δv of 21.7 m/s (26.2% less) and the total flight time is longer than the typical rendezvous by 4.9%.

CONCLUSIONS

Algorithms and operations concepts have been presented for ensuring safety during a spacecraft circumnavigation mission. These techniques are also applicable to a wide range of other spacecraft proximity operations missions, including rendezvous. The inspection mission described in this paper is very useful for space situational awareness and spacecraft health verification. Additionally, any mission requiring one spacecraft to service another will first require the servicing spacecraft to safely close distance and operate for a period of time in proximity to the spacecraft to be serviced. Furthermore, a wide variety of spacecraft science missions have been proposed that rely on small spacecraft operating in close proximity to each other, and any such mission can benefit from the algorithms and operations concepts presented.

Ongoing safe spacecraft proximity research includes the simulation of the circumnavigation mission in a high-fidelity hardware-in-the-loop simulation environment that includes the effects of non-linearity, space environment perturbations, and realistic navigation errors. Additionally, design efforts are underway, with promising initial results, for a controller capable of achieving all the trajectories described in this paper in the presence of non-linearity, perturbations, and navigation error.

REFERENCES

1. Foster, J. L. and Estes, H. S. "A Parametric Analysis of Orbital Debris Collision Probability and Maneuver Rate for Space Vehicles," NASA JSC 25898, August 1992.

2. Khutorovsky, Z.N., Boikov, V., and Kamensky, S.Y. "Direct Method for the Analysis of Collision Probability of Artificial Space Objects in LEO: Techniques, Results, and Applications," Proceedings of the First European Conference on Space Debris, ESA SD-01, 1993, pp. 491 -508.

3. Carlton-Wippern, K. C. "Analysis of Satellite Collision Probabilities Due to Trajectory and Uncertainties in the Position/Momentum Vectors," *Journal of Space Power*; Vol. 12, No. 4, 1993.

4. Chan, K. F. "Collision Probability Analyses for Earth Orbiting Satellites," *Advances in the Astronautical Sciences*, Vol. 96, 1997, pp. 1033- 1048.

5. Brend, N. "Estimation of the Probability of Collision Between Two Catalogued Orbiting Objects," *Advances in Space Research*, Vol. 23, No. 1, 1999, pp. 243-247.

6. Oltrogge, D. and GIST, R. "Collision Vision Situational Awareness for Safe and Reliable Space Operations," 50th International Astronautical Congress, October 4-8, 1999, Amsterdam, The Netherlands, IAA-99-IAA.6.6.07.

7. Akella, M. R. and Alfriend, K. T. "Probability of Collision Between Space Objects," *Journal of Guidance, Control, and Dynamics*, Vol. 23, No. 5, September-October 2000, pp. 769-772.

8. Chan, K.F. "Analytical Expressions for Computing Spacecraft Collision Probabilities," AAS/AIAA Space Flight Mechanics Meeting, Santa Barbara, California, February 1 1 - 15, 2001.

Patera, R. P. "General Method for Calculating Satellite Collision Probability," *Journal of Guidance, Control, and Dynamics*, Volume 24, Number 4, July-August 2001, pp. 716-722.

9. Bryson and Ho, Applied Optimal Control, Taylor & Francis Publishing, 1st Ed., 1975, p. 311.

10. Naasz, Bo, "Safety Ellipse Motion with Coarse Sun Angle Optimization," NASA GSFC Flight Mechanics Symposium, Greenbelt, MD, October 18-20, 2005.